Redox reactions, radio-photoluminescence and thermoluminescence in $CaSO_4:Eu$

1997 J. Phys.: Condens. Matter 9 8307

(http://iopscience.iop.org/0953-8984/9/39/015)

J. Phys.: Condens. Matter **9** (1997) 8307–8323. Printed in the UK PII: S0953-8984(97)82562-3

Redox reactions, radio-photoluminescence and thermoluminescence in $CaSO_4$:Eu

S R Nair†, V K Kondawar†, S V Upadeo‡, S V Moharil‡ and T K Gundurao§

† National Environmental Engineering Research Institute, Nagpur, India
‡ Department of Physics, Nagpur University, Nagpur 440 010, India
§ RSIC, Indian Institute of Technology, Powai, Mumbai 400076, India

Received 13 March 1997, in final form 2 July 1997

Abstract. $CaSO_4$:RE phosphors find applications in dosimetry of ionizing radiations. Phosphors having Dy or Tm activators are high-sensitivity thermoluminescence dosimetry materials, while the phosphors with Eu or Sm activators are the proposed materials for radio-photoluminescence dosimetry. Mechanisms of several processes related to various luminescence phenomena, however, are not yet properly understood. Usually, all $CaSO_4$:RE phosphors are prepared under identical conditions and comparative studies are carried out. It is shown here that the form in which the impurity is incorporated and the nature of defects produced is quite different in $CaSO_4$:Eu than in $CaSO_4$:Dy. The results presented throw light on the mechanism for thermoluminescence, radio-photoluminescence, incorporation of the impurity and $Eu^{3+} \leftrightarrow Eu^{2+}$ conversion.

1. Introduction

Rare earth (RE) doped $CaSO_4$ phosphors have been studied for quite some time (Azorin *et al* 1993). Dy (Yamashita *et al* 1968, 1971) and Tm (Yamashita 1974) are known to be efficient activators for thermoluminescence (TL) in a $CaSO_4$ host. $CaSO_4$:Eu and $CaSO_4$:Sm were found to exhibit interesting photoluminescence (PL) properties and the possibility of using these phosphors in radio-photoluminescence (RPL) dosimetry (Calvert and Danby 1984) and UV dosimetry using TL (Danby 1988) was indicated. While studying $CaSO_4$:RE phosphors, usually phosphors corresponding to various RE impurities have been prepared in a similar way, keeping the preparation conditions, impurity concentrations, etc identical (Nambi *et al* 1974). Similar models have been proposed to explain the thermoluminescence in all the $CaSO_4$:RE phosphors. Nambi *et al* (1974) extended the model based on the redox reactions proposed by Merz and Pershan (1967a, b) for CaF_2:RE phosphors. According to this model, exposure to ionizing radiations results in $RE^{3+} \rightarrow RE^{2+}$ conversion and trapped hole centres. During heating, holes are detrapped and they recombine with RE^{2+} to give RE^{3+} in an excited state. Radiative de-excitation to the ground state leads to TL emission. (This will be referred to as model I.) Borrowing from the terminology used in chemistry, $RE^{3+} \leftrightarrow RE^{2+}$ conversions have been called redox reactions. Nambi *et al* (1974) also suggested another model, which was later supported by Morgan and Stoebe (1986, 1989, 1990). This model proposed that there is no direct recombination at the RE site, but the energy of electron–hole recombination is transferred to RE^{3+}. (This will be referred to as model II.) Thus model I assigns an important role in the TL mechanism to redox reactions,

0953-8984/97/398307+17$19.50

while for model II these reactions are not directly relevant. Yet another application of the redox reactions in the field of radiation dosimetry was envisaged. For several RE impurities (e.g. Eu and Sm), RE^{2+} and RE^{3+} yield characteristically different PL. Redox reactions will thus lead to RPL. Use of $CaSO_4$:Eu or Sm for RPL dosimetry was proposed by Calvert and Danby (1984). However, it was found that not all the RE^{2+} produced during exposures to ionizing radiations returns to RE^{3+}. This poses a serious hurdle in the way of reusability of such phosphors. The reason for the incomplete back-conversion is not clear.

In recent years Moharil and co-workers have reported several experiments on Eu doped samples which showed lack of correlation between redox reactions and TL (Dhopte *et al* 1991a, b, 1992, Atone *et al* 1993a, Upadeo *et al* 1994, Upadeo and Moharil 1995). During these investigations we found that $CaSO_4$:Eu system can be more complicated (Dhopte *et al* 1991b), in that, depending upon the method of preparation and the thermal history, Eu may be in divalent or trivalent form. The need for a more detailed study of this phosphor was indicated. In this paper we report results of investigations on various $CaSO_4$:Eu phosphors aimed at explaining the mechanism of TL and RPL. The results show that, contrary to the assumptions of previous studies, $CaSO_4$:Eu phosphor behaves quite differently from $CaSO_4$:Dy phosphor. In most of the previous studies, Eu related centres have been studied through PL but the nature of the defects in the anionic sub-lattice has not been investigated. It had been presumed that the trapped hole centres in all $CaSO_4$:RE phosphors would be similar. A detailed study of trapped hole centres in $CaSO_4$:Eu using the electron spin resonance (ESR) technique was also made.

2. Experimental details

$CaSO_4$:Eu samples can be prepared with Eu impurity in the desired valence state. In the first method, which leads to samples with Eu in predominantly divalent form, typically, $CaCl_2.2H_2O$ (7.35 g Analar grade) was dissolved in triply distilled deionized water. $EuCl_2$ (11.4 mg) was added to the solution. $CaSO_4$:Eu was precipitated by addition of H_2SO_4 (GR grade, Merck). The precipitate was collected and dried in an oven at 373 K and then it was annealed at 673 or 973 K. These samples will be denoted as P-400 and P-700, the number indicating the annealing temperature in degrees Celsius.

To prepare the sample free of Eu^{2+} the procedure used by Danby (1988) was adopted. Typically, $Ca(NO_3)_2.4H_2O$ (2.36 g) and Eu_2O_3 (3.5 mg) were dissolved in about 50 ml concentrated H_2SO_4. Acid was distilled out in a close system similar to that used for the preparation of the dosimetry phosphor $CaSO_4$:Dy (Iyer *et al* 1980). $CaSO_4$:Eu thus prepared was repeatedly washed with distilled water to remove the traces of acid and dried in an oven at 373 K. These samples will be designated as samples D.

TL glow curves were recorded with the usual set-up consisting of a small metal plate heated directly using a temperature programmer, photomultiplier (931 B), d.c. amplifier and millivolt recorder. 5 mg phosphor was heated every time at the rate of 150 K min^{-1}.

A Co^{60} source was used to expose the samples to gamma rays. Fluorescence from various irradiated and unirradiated samples was studied on a Hitachi F-4000 fluorescence spectrophotometer. The same amount of sample was used every time. Emission and excitation spectra were recorded using a spectral slit width of 1.5 nm.

ESR measurements were carried out on a Varian E-112, E-line Century Series, X-band ESR spectrometer which utilizes 100 kHz field modulation. TCNE ($g = 2.002\,77$) was used as a standard for g-factor measurements.

UV exposures were performed using an Ultra-Violet Product model UVG-54 lamp.

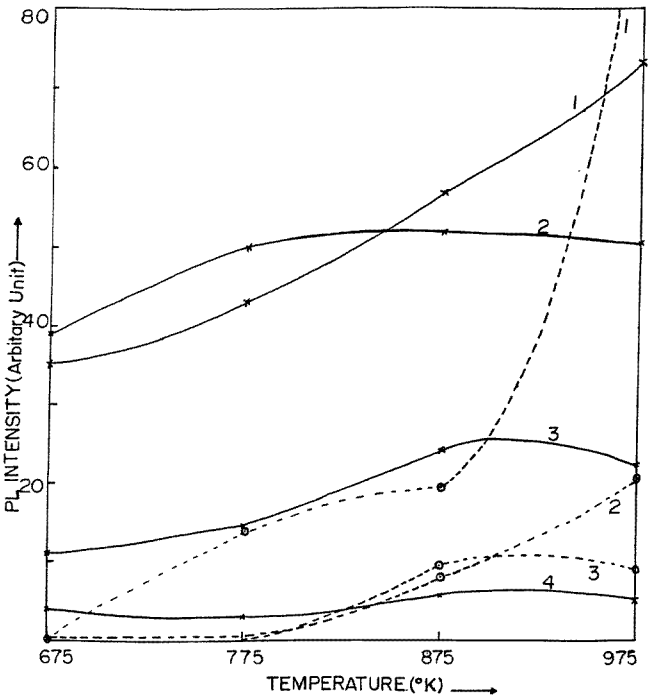

Figure 1. The effect of annealing on incorporation of Eu in $CaSO_4$: PL intensities of Eu^{2+} (dashed) and Eu^{3+} (solid) are plotted as functions of annealing temperature in various $CaSO_4$:Eu samples. Eu concentrations (mol%): 1, 0.1; 2, 0.05; 3, 0.005; 4, 0.0005.

3. Results and discussion

3.1. Incorporation of Eu

In the case of $CaSO_4$:Dy or Tm, impurity concentrations in the range 0.05–0.2 mol% were found to be optimum for TL (Ayyangar *et al* 1974, Nambi *et al* 1974, Prokic 1978, Atone *et al* 1993b). While studying redox reactions and RPL in $CaSO_4$:Eu, similar concentrations have been used in previous studies (Bapat 1977, Calvert and Danby 1984, Upadeo *et al* 1994). We found that the solubility of Eu^{3+} in $CaSO_4$ is quite low. The presence of Eu^{3+} can be identified in PL in the form of emission lines around 595 and 610 nm corresponding to $^5D_0 \rightarrow {}^7F_2$, $^7F_1$ transitions. PL emission of Eu^{2+}, on the other hand, is in the form of a narrow band around 390 nm corresponding to transitions between the lowest band of the $4f^65d^1$ configuration and the ground state $^8S_{7/2}$ of the $4f^7$ configuration. Figure 1 shows the intensity of Eu^{2+} and Eu^{3+} PL as a function of annealing temperature in unirradiated samples D for various Eu concentrations. It is seen that for low concentration (5 ppm), no Eu^{2+} PL is detectable up to an annealing temperature of 700 °C. For higher concentration, Eu^{2+} emission becomes observable at high enough annealing temperature. For concentration of 0.1 mol%, Eu^{2+} PL is observable for annealing temperatures above 400 °C. However, it may be noted that there is no significant decrease in Eu^{3+} emission. Thus, Eu^{2+} is not obtained by thermal conversion of Eu^{3+} as had been suggested in the previous study (Dhopte *et al* 1991b). It is apparent that, in the as-prepared samples, Eu exists as Eu^{3+} or some non-luminescent aggregated form. During thermal annealing the aggregates break to give

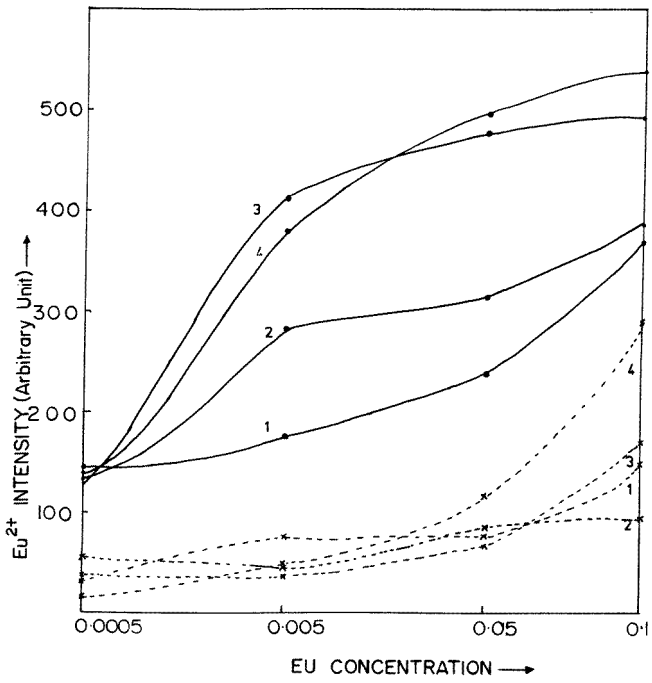

Figure 2. The dependence of $Eu^{3+} \leftrightarrow Eu^{2+}$ conversion on Eu concentration. The intensity of Eu^{2+} PL in samples exposed to 5.22 C kg^{-1} (solid curves) and then annealed (broken curves) is plotted as a function of Eu concentration for various pre-annealing temperatures. Pre-annealing temperatures (K): 1, 673; 2, 773; 3, 873; 4, 973.

Eu^{3+} and Eu^{2+}; higher concentrations and annealing temperatures favouring Eu^{2+} formation. This explains the better formation of Eu^{2+} in precipitated samples than in samples D. Eu remains in aggregate form in the precipitated samples. Thermal breaking up of aggregates leads to higher concentrations of Eu^{2+}. In samples D, more Eu is incorporated in the Eu^{+3} form, and thus during heating, when Eu^{2+} is obtained by breaking up of aggregates, fewer Eu aggregates are available. Thus, we find that the amount of Eu that can be incorporated as Eu^{3+}, without introducing Eu^{2+}, is less than 0.005 mol%, which is far below the concentrations of the order of 0.1 mol% used in the previous studies. There is no thermal $Eu^{3+} \rightarrow Eu^{2+}$ conversion, but it is the undissolved Eu which is dispersed in the form of Eu^{2+}, when higher annealing temperatures are used for dispersion.

3.2. Radiation induced $Eu^{3+} \leftrightarrow Eu^{2+}$ conversion

Figure 2 shows the concentration dependence of Eu^{2+} PL in samples D exposed to gamma rays at 5.22 C kg^{-1}. For low annealing temperature (400 °C) Eu^{2+} PL intensity increases monotonically with Eu concentration, while for higher annealing temperatures the increase is prominent in the concentration range 5–50 ppm (5×10^{-4}–5×10^{-3} mol%). Obviously not all the Eu^{2+} is obtained from radiation induced $Eu^{3+} \rightarrow Eu^{2+}$ conversion; part of it is obtained by breaking of aggregates by exposure to gamma rays. This is evident from the fact that after post-irradiation annealing there is no complete $Eu^{2+} \rightarrow Eu^{3+}$ back-conversion (figure 2, dashed curves). Maximum back-conversion is obtained up to concentrations of 50 ppm and annealing temperature 600 °C. Under these conditions, one has obtained

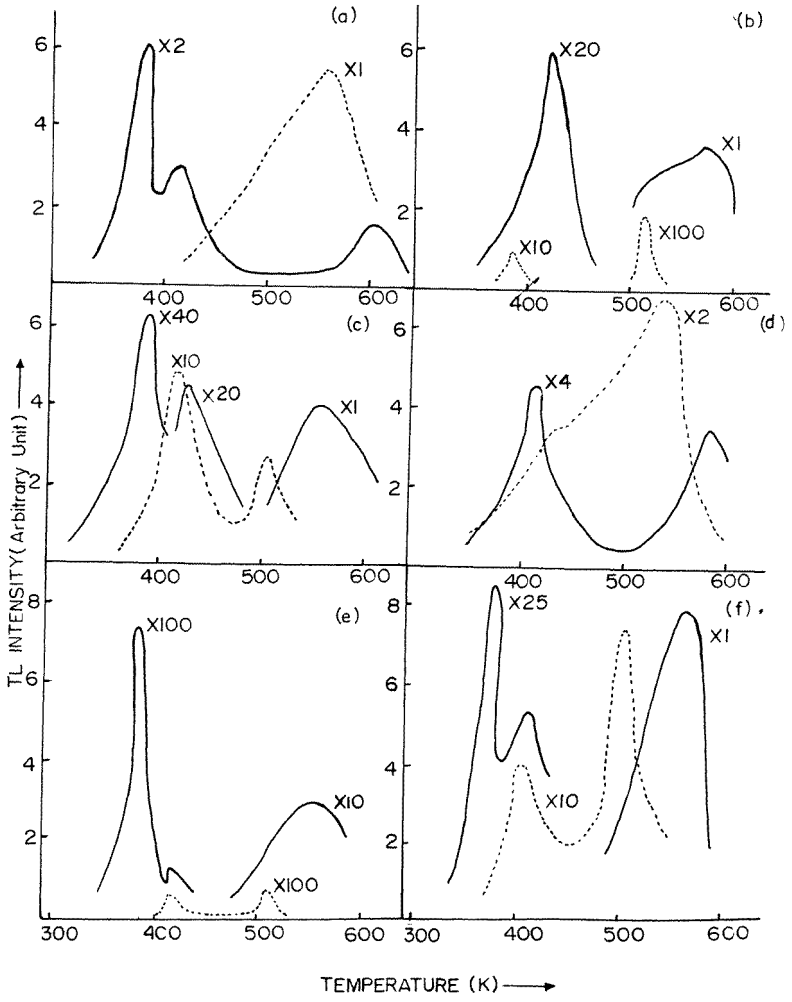

Figure 3. Typical glow curves for various $CaSO_4$ samples exposed to gamma rays (0.2 C kg^{-1}, solid curves) or UV (dashes). Numbers on the curves are the multipliers of the ordinates for obtaining relative intensities. (a) $CaSO_4$:Gd (0.02), Eu (0.002); (b) $CaSO_4$:Eu (0.005); (c) $CaSO_4$:Rb (0.1), Eu (0.002); (d) $CaSO_4$:Y (0.02), Eu (0.002); (e) $CaSO_4$:K (0.1), Eu (0.01); (f) $CaSO_4$:La (0.05), Eu (0.005).

an optimum amount of Eu^{3+} dispersed in the host, without introducing Eu^{2+} or leaving aggregates. Above this concentration, and for lower annealing temperatures, part of the Eu exists in aggregate form. During the irradiation aggregates break to yield Eu^{2+}. During post-irradiation thermal annealing, Eu^{2+} obtained from $Eu^{3+} \rightarrow Eu^{2+}$ conversion goes back to the Eu^{3+} form, while that obtained by breaking up of the aggregate stays as Eu^{2+}. This explains the incomplete $Eu^{2+} \rightarrow Eu^{3+}$ back-conversion during the post-irradiation annealing, which is detrimental to application in RPL dosimetry (Calvert and Danby 1984, Dhopte *et al* 1991b). This also suggests that the $Eu^{2+} \rightarrow Eu^{3+}$ back-conversion during post-irradiation thermal annealing is a localized process. Only those Eu^{2+} ions which have been converted by reduction of Eu^{3+} by irradiation and thus having hole centres in their vicinity can go back to Eu^{3+} by capturing a hole. Eu^{2+} ions obtained by breaking up of

aggregates and not having holes in their vicinity remain in the same valence state, even after the post-irradiation annealing.

3.3. Effect of co-dopants on $Eu^{2+} \rightarrow Eu^{3+}$ back-conversion

Complete back-conversion of Eu^{2+} to Eu^{3+} is important for obtaining reusable samples for applications in RPL dosimetry. As the results of the previous sections suggest that the incomplete back-conversion is due to the presence of Eu aggregates and their breaking up into Eu^{2+} by irradiation, it was considered that dispersion of Eu^{3+} by charge compensation may lead to better back-conversion. $CaSO_4$:Eu samples with monovalent cationic co-dopants as charge compensators were thus prepared. Samples obtained with various impurity concentrations and annealing temperatures were studied. Results are presented for the samples exhibiting best back-conversion. Table 1 gives the relative intensity of Eu^{2+} PL in various samples (column 1) exposed to gamma rays (5.9 C kg^{-1}), and then given the post-irradiation annealing treatment (last column). It is seen that in $CaSO_4$:K, Eu there is optimum $Eu^{3+} \leftrightarrow Eu^{2+}$ conversion. However, even in this sample there is no complete $Eu^{2+} \rightarrow Eu^{3+}$ back-conversion.

Table 1. Correlation (or lack of correlation) between $Eu^{3+} \leftrightarrow Eu^{2+}$ conversion and TL data obtained for various $CaSO_4$ samples.

Dopant	1	2	3	4
Gd (0.02), Eu (0.002)	62	5.5	2.9	18
Y (0.02), Eu (0.002)	84	14.0	9.9	21
Rb (0.1), Eu (0.002)	210	22.5	4.1	27
La (0.05), Eu (0.005)	366	42.0	7.1	25
Eu (0.05)	381	217.0	3.1	74
K (0.1), Eu (0.01)	506	76	3.1	23

1. Intensity of Eu^{2+} PL in samples exposed to gamma rays.
2. Intensity of the high-temperature glow peak in the glow curve of the UV exposed samples (relative units).
3. Intensity of the high-temperature glow peak in the glow curve of the samples exposed to gamma rays (relative units).
4. Intensity of Eu^{2+} PL in samples exposed to gamma rays and then annealed at 600 °C, 15 min.

Other rate earth impurities such as La, Gd and Y were also tried as co-dopants. It is known that Eu is retained in trivalent form in La, Gd and Y hosts (Upadeo and Moharil 1997). There is better back-conversion in these samples as compared to the sample doped with only Eu. However, the RPL intensity is less in the samples with Y or Gd as co-dopants.

3.4. Thermoluminescence measurements

Figure 3 shows glow curves for various samples exposed to gamma rays. In all the samples dominant glow peaks appear around 383 and 415 K. A weaker glow peak can also be observed around 560 K.

According to model I irradiation produces trapped hole centres and reduction of Eu^{3+} to Eu^{2+}. TL emission is obtained in the form of characteristic Eu^{3+} emission when a thermally released hole recombines with Eu^{3+}. This suggests that TL intensity should be correlated to $Eu^{3+} \leftrightarrow Eu^{2+}$ conversion, and after heating past the glow peak $Eu^{2+} \rightarrow Eu^{3+}$ back-conversion should take place. We have earlier shown (Upadeo *et al* 1994) that the peaks at

lower temperatures are not correlated with $Eu^{2+} \rightarrow Eu^{3+}$ back-conversion. Further evidence showing lack of correlation between TL and $Eu^{2+} \rightarrow Eu^{3+}$ conversion is now presented. Figure 4 shows intensities of various glow peaks as a function of Eu concentration. The intensity of RPL as a function of Eu concentration is also shown for comparison. It is seen that while the RPL intensity increases in the Eu concentration range 5–50 ppm, intensities of lower-temperature peaks decrease. The glow peak around 560 K is more intense at higher Eu concentrations. However, it is also not correlated to $Eu^{3+} \rightarrow Eu^{2+}$ conversion. In table 1 the intensity of this peak and RPL intensity in various samples are given. There is no correlation between these quantities. Thus, none of the glow peaks in the gamma irradiated samples seem to be correlated with $Eu^{3+} \leftrightarrow Eu^{2+}$ conversion.

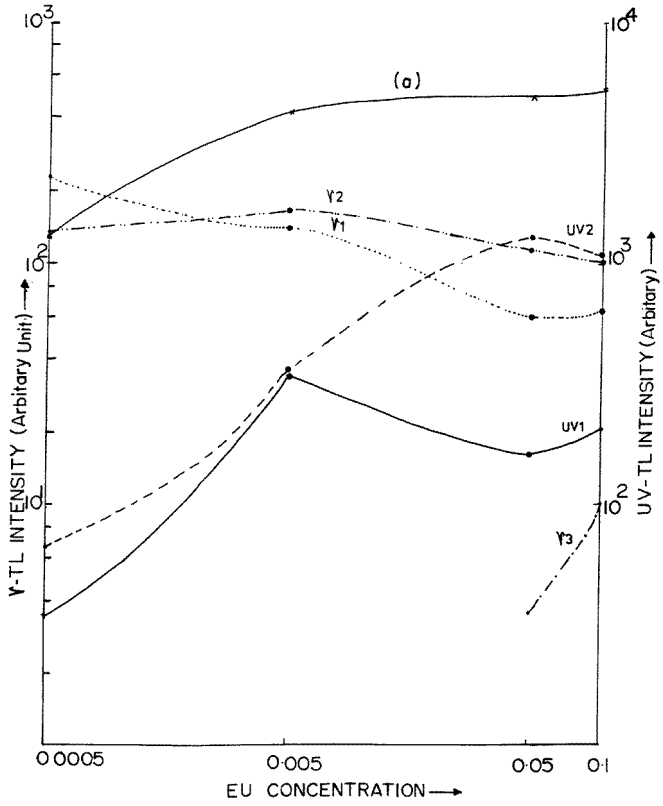

Figure 4. The effect of Eu concentration on intensity of TL glow peaks. Heights of various peaks in the glow curves are plotted as a function of Eu concentration. A similar dependence of PL on Eu^{2+} obtained by irradiation induced oxidation of Eu^{3+} is also plotted for reference (curve a). The lack of correlation is obvious. Glow peaks in the gamma irradiated (0.17 C kg^{-1}) samples: γ_1, 373 K; γ_2, 413 K; γ_3, 560 K. Glow peaks in the UV exposed samples: UV_1, 383 K; UV_2, 480 K.

In our earlier work we have presented results which suggested that the mechanisms of UV induced TL and gamma induced TL could be different. The high-temperature peak is more dominant in UV exposed samples than in the samples exposed to gamma rays. Results on TL in samples exposed to UV are included in figures 3 and 4 and table 1. In the samples doped with Eu alone, the dependence of RPL and high-temperature glow peak on the Eu concentration show some correlation. In the co-doped samples UV induced TL

is weaker, but again there is good correlation between RPL intensity and the intensity of the high-temperature glow peak (columns 1 and 2, table 1). There is no such correlation between RPL and the high-temperature peak in the gamma irradiated samples (columns 1 and 3, table 1). From these data it seems that model I may be valid for the high-temperature peak in the UV exposed samples. This glow peak may originate in the redox reactions.

3.5. ESR measurements

Eu^{2+} shows characteristic ESR signal and thus ESR measurements can be useful in studying $Eu^{3+} \rightarrow Eu^{2+}$ conversion. Some of the trapped hole centres such as SO_4^- and SO_3^- can also be detected by ESR (Danby *et al* 1982, Danby 1983, Danby and Mason 1984). ESR measurements on various $CaSO_4$ samples showed that the nature of the hole centres produced in Eu doped samples is different from that observed in the dosimetry phosphor $CaSO_4$:Dy. TL related centres in $CaSO_4$:Dy are SO_4^- radicals. ESR signals in $CaSO_4$:Eu samples can be assigned to SO_4^- and SO_3^- radicals in different local environments, as will be shown in the following. In various $CaSO_4$:Eu samples relative concentrations of these centres differ. First we describe the type of trapped hole centre studied through ESR in various ESR samples and then we describe the dependence of the relative concentration of various types of hole centres on the method of preparation.

Figure 5 shows the ESR spectrum of $CaSO_4$:Eu recorded at 25 °C after exposure to gamma rays. The scan range has been selected to record only the lines in the vicinity of free electron resonance. There are several lines in the spectrum and the lines labelled as A–C have been assigned to three distinct defect centres. The line A is characteristic of a centre exhibiting a nearly isotropic g-tensor with principal value 2.0108. This centre is assigned to an SO_4^- radical.

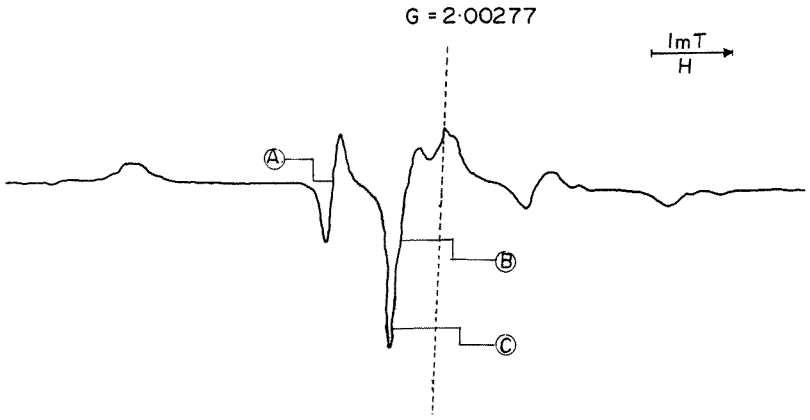

Figure 5. The ESR spectrum of gamma irradiated $CaSO_4$:Eu recorded at room temperature.

Several SO_4^- centres are observed in pure and doped $CaSO_4$ and the g values of these centres are given in table 2. The SO_4^- radical assigned to line A in the present study has close similarities to the corresponding radical observed by Huzimura in pure $CaSO_4$. In this study, precise measurements showed that the g tensor has slight axial symmetry with principal values $g_\perp = 2.012$ and $g_\parallel = 2.011$. This feature will be discussed later in relation to the low-temperature SO_4^- radical observed in the present study.

Table 2. Principal g values reported for radiation induced SO_4 radicals in $CaSO_4$ and doped $CaSO_4$ lattices.

Material	Temperature (K)	g values	Reference
$CaSO_4$	300	$g_\parallel = 2.011 \simeq g_\perp = 2.012$	Huzimura (1979)
$CaSO_4$:Tm	300	2.011, 2.022, 2.005	Huzimura *et al* (1980)
$CaSO_4$:Tm	300	2.004, 2.012, 2.028	Huzimura and Atarashi (1982)
$CaSO_4$:Tm	300	2.009, 2.020	Huzimura and Atarashi (1982)
$CaSO_4$:Dy	120	2.0006, 2.0091, 2.0395	Danby *et al* (1982)
$CaSO_4$:Sm	77	$g_\parallel = 2.0288$, $g_\perp = 2.0101$	Sheshagiri *et al* (1988)
$CaSO_4$:Sm	300	$g_\parallel = 2.0263$, $g_\perp = 2.0144$	Sheshagiri *et al* (1988)
$CaSO_4$:^{241}Am	77	$g_\parallel = 2.0370$, $g_\perp = 2.0060$	Natarajan *et al* (1988)
$CaSO_4$:^{241}Am	300	$g_\parallel = 2.0260$, $g_\perp = 2.0106$	Natarajan *et al* (1988)
$CaSO_4$:Dy	77	2.0022, 2.0081, 2.0386	Morgan and Stoebe (1990)
$CaSO_4$:Dy, Na	300	$g_\parallel = 2.0060$, $g_\perp = 2.0113$	Gundu Rao *et al* (1993)

The SO_4^- defect centre is a hole trap centre. The trapping of a hole at an SO_4^{2-} ion leads to the formation of an SO_4^- centre. We have optimized the geometry of the SO_4^- radical using the gradient optimization method. The S–O_1 bond is found to be 1.66 Å whilst the other three S–O lengths are 1.53 Å. OSO angles are found to be 103°. The calculated atomic charges using the MNDO method (Dewar and Thiel 1977) show that the positive charge of the trapped hole is localized predominantly on one of the oxygen atoms (O_1). In the $CaSO_4$ lattice, a stable charge distribution of the SO_4^- radical is possible if the SO_4^- centres are preferentially forming near Ca^{2+} vacancies. The excess negative charge present at such a vacancy is partially cancelled by the positive hole on SO_4^- centre. SO_4^- radicals observed in $CaSO_4$:Dy by Danby *et al* (1982) and Morgan and Stoebe (1990) would correspond to a situation of this kind. On the other hand, the excess negative charge of the Ca^{2+} vacancy would be completely cancelled by the formation of two hole centres at the SO_4^- ion. This corresponds to a more stable configuration and such hole centres have been observed by Morgan and Stoebe (1990) in $CaSO_4$:Dy single crystals.

The extent of neutralization of the excess negative charge at the cation vacancy seems to decide the degree of distortion of the SO_4^- tetrahedron from T_d symmetry. Relatively considerable deviations from tetrahedral symmetry are indicated by the large g shifts observed for the SO_4^- centre in the $CaSO_4$:Dy system (table 2). However, there appears to be not much distortion of the SO_4^- tetrahedron for the radical observed in $CaSO_4$:Dy, Na. Here, the SO_4^- radical is stabilized by the Na^+ ion occupying the Ca^{2+} site. Na^+ in V_{Ca} has an excess negative charge which is completely neutralized by the hole on the SO_4^- radical. This is in contrast with the [V_{Ca}–SO_4^-] case ($CaSO_4$:Dy, where the positive hole is not able to neutralize completely the negative charge at the V_{Ca} site. The lesser degree of distortion in the $CaSO_4$:Dy, Na system is reflected in the axial nature of the g tensor and relatively small g shifts. In the present study, the g shifts are not very large and also the g tensor is nearly isotropic in contrast with many of the observed SO_4^- radicals (table 2).

Bishop *et al* (1966) and Samoilovich *et al* (1968) have discussed the electronic structure of the SO_4^- radical on the basis of semiempirical molecular orbital calculations assuming tetrahedral T_d symmetry for the molecule. More accurate *ab initio* SCF calculations have been carried out by Johansen (1974). These studies yield the following electronic configuration for the 31-valence-electron SO_4^- ion:

$$(1a_1)^2(1t_2)^6(2a_1)^2(2t_2)^6(1e_4)^4(3t_2)^6(1t_1)^5 \qquad {}^2T_1.$$

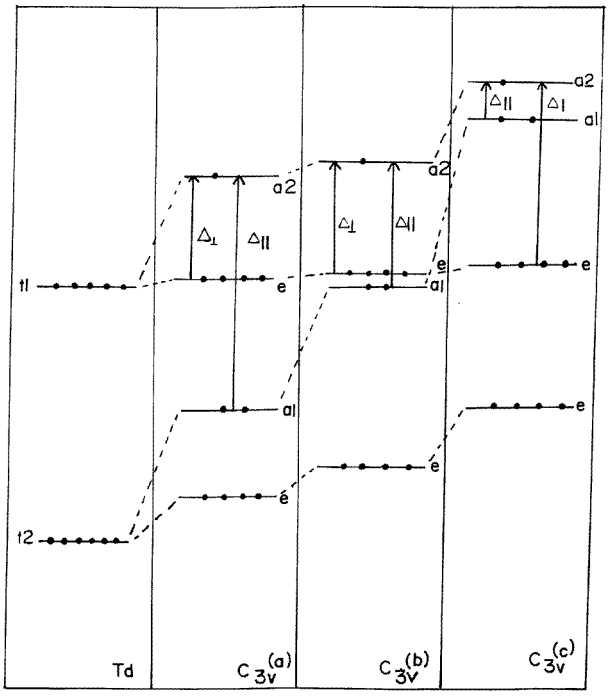

Figure 6. The orbital level scheme for the SO_4^- ion showing the correlation between T_d and C_{3v} symmetries. $C_{3v}^{(a)}$ refers to a small reduction in symmetry from T_d while $C_{3v}^{(b)}$ and $C_{3v}^{(c)}$ correspond to larger distortions from T_d symmetry.

Thus, the SO_4^- radical is expected to have a $^2T_1$ ground state with the unpaired electron confined to ligand atoms. The $^2T_1$ tetrahedral spatial configuration is intrinsically unstable (Atkins and Symons 1967). Although distortion from the tetrahedral T_d symmetry could follow from this instability, it could also be imposed by an unsymmetrical environment such as a non-spherical distribution of adjacent cations.

As mentioned earlier, the SO_4^- centre in the present case appears to be stabilized by a nearby Ca^{2+} vacancy. In the $CaSO_4$:Dy, Na system there is more efficient compensation of the excess negative charge present at the $V_{Ca}(Na^+)$ site due to the hole on the SO_4^- ion. As such there will be less reduction in symmetry of the SO_4^- tetrahedron from T_d symmetry. However, there is likely to be more distortion in the present case in contrast to the $CaSO_4$:Dy, Na system due to less neutralization of the excess negative charge at the cation vacancy. C_{3v} and C_{2v} point groups may be considered for the SO_4^- ion and the former is assumed based on the present ESR results which show a nearly isotropic g tensor.

The orbital energy diagram for the SO_4^- ion and the changes on going from T_d to C_{3v} symmetry are shown in figure 6. The degree of distortion depends not only on the extent of charge neutralization at the cation vacancy but also on the local environment of the SO_4^- ion. We have, therefore, considered three possibilities for the C_{3v} symmetry case depending upon the degree of distortion. These are shown as $C_{3v}^{(a)}$, $C_{3v}^{(b)}$ and $C_{3v}^{(c)}$ in figure 6. Only relevant orbitals are shown for simplicity and excitations for the g shifts are also indicated.

In C_{3v} symmetry, the g shifts for the SO_4^- ion are qualitatively understood as follows.

The perpendicular value $g_\perp$ arises from the excitation

$$\ldots(e)^4(a_1)^2(e)^3(a_2)^2, {}^2E \leftarrow (e)^4(a_1)^2(e)^4(a_2)^1, {}^2A_2$$

and the parallel value $g_\parallel$ from the excitation

$$\ldots(e)^4(a_1)^1(e)^4(a_2)^2, {}^2A_1 \leftarrow (e)^4(a_1)^2(e)^4(a_2)^1, {}^2A_2.$$

The closed e level is seen in the orbital energy diagram to lie close to and beneath the a_2 level (figure 6, $C_{3v}^{(a)}$). Consequently, the perpendicular g value should be larger than the free-spin value. On the other hand, the a_1 level is a little further below the a_2 level and the parallel g value should be closer to the free-spin value. The unpaired electron in the a_2 orbital is confined to the ligand atoms and is expected to have only a small hyperfine interaction with the nucleus of the central atom. It thus appears that the SO_4^- radical will have a spectrum characterized by a g tensor which exhibits axial symmetry with $g_\perp > g_\parallel$ and a small hyperfine interaction with the central nucleus. These expectations are well borne out by the experimental observations in the $CaSO_4$:Dy, Na system (Gundu Rao *et al* 1993).

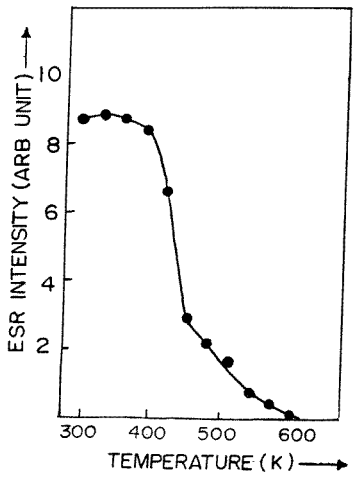

Figure 7. The thermal stability of the SO_4^- (A) radical in $CaSO_4$:Eu.

The distortion of the SO_4^- ion from T_d symmetry is small in the above discussion. In the present case, where the SO_4^- radical is stabilized by a nearby Ca^{2+} vacancy, the distortion is likely to be larger as the excess negative charge on the vacancy is only partially cancelled by the hole on the radical. For simplicity, it is assumed that the radical still has C_{3v} symmetry. The changes in the energies of the relevant orbitals are shown in figure 6, $C_{3v}^{(b)}$. The unpaired electron still occupies the a_2 orbital and the ^{33}S hyperfine interaction (the major isotope ^{32}S is non-magnetic) is expected to be small. The ground state is A_2 and the relevant excited states are A_1 and E for $g_\parallel$ and $g_\perp$ shifts respectively. It is seen from the orbital level scheme (figure 6) that a_1 and e levels are close to each other and lie below and close to the a_2 level. Hence, $g_\perp$ is expected to be large compared to the free-spin value and at the same time nearly the same as the $g_\parallel$ value, as the energy difference of a_1 and e levels is nearly the same. The present experimental observations for the SO_4^- radical are in accordance with these expectations. It is observed that $g_\perp \simeq g_\parallel$ in marked constant with most of the SO_4^- radicals observed in the literature and also with the SO_4^- radical stabilized by an Na^+ ion ($g_\parallel < g_\perp$). These differences arise because of changes in the energies of orbitals owing to difference in the degree of distortion of the SO_4^- ion from T_d symmetry.

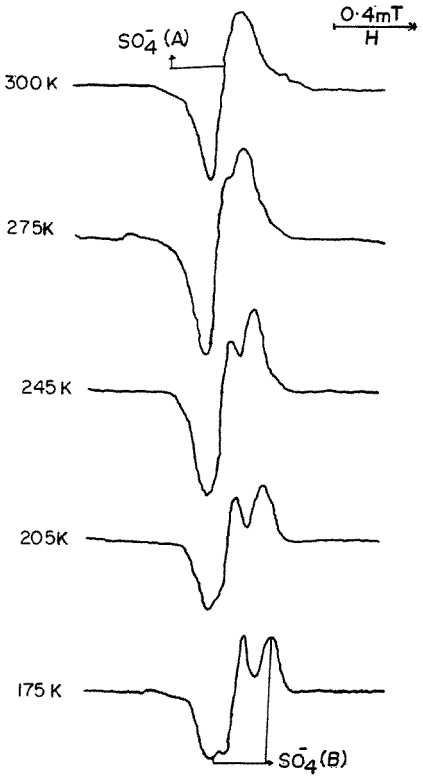

Figure 8. The ESR spectrum of the SO_4^- (A) radical and the appearance of the SO_4^- (B) radical with lowering of temperature.

The stability of the SO_4^- ion was measured using a step annealing technique. The sample was returned to room temperature and the ESR signal intensity was measured after each step. Figure 7 shows the thermal decay of the SO_4^- (A) centre. These measurements show that the SO_4^- (A) radical begins to decay from 373 K and from this temperature onwards the rate of decay is large and continues until 453 K. The SO_4^- (A) centre releases holes during this decay and, as the range of decay corresponds approximately to the glow peak temperature range, it is likely that the 413 K TL peak observed in $CaSO_4$:Eu samples may be caused by the holes released from this centre.

The ESR line from the SO_4^- (A) radical showed a small asymmetry in its line shape. With a view to examining the line shape and a possible increased resolution, the SO_4^- (A) radical was examined at various low temperatures. These experiments showed a growth of a new radical at almost the same position as the SO_4^- (A) centre. Figure 8 shows the growth of this radical with lowering temperature. This centre is characterized by an axial g tensor with principal values $g_\parallel = 2.0115$ and $g_\perp = 2.0103$ and is also assigned to a SO_4^- centre (labelled as SO_4^- (B)). The principal g values of this centre are in accordance with the g factors for most of the observed SO_4^- radicals (table 2) and would correspond to a situation where the SO_4^- tetrahedron is slightly more distorted than the SO_4^- (A) centre. Step annealing measurements show that the SO_4^- (B) centre decays in the temperature range 353–423 K. Figure 9 shows the thermal stability of the SO_4^- (B) centre. It is seen that the decay temperature range of SO_4^- (B) correlates reasonable well with the TL glow peak

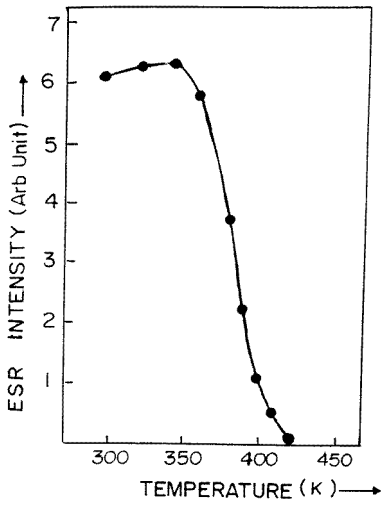

Figure 9. The thermal stability of the SO_4^- (B) radical in $CaSO_4$:Eu.

Table 3. Principal g values reported for radiation induced SO_3^- centres in pure and doped $CaSO_4$ lattices.

Material	Temperature (K)	g values	Reference
$CaSO_4$	300	2.0048, 2.0038, 2.0029 (I)	Huzimura (1979)
$CaSO_4$	300	2.0050, 2.0035, 2.0018 (II)	Huzimura (1979)
$CaSO_4$:Tm	300	2.0011, 2.0021, 2.0051 (I)	Huzimura *et al* (1980)
$CaSO_4$:Tm	300	2.0037 (II)	Huzimura *et al* (1980)
$CaSO_4$:Tm	300	2.0010, 2.0020, 2.0060 (I)	Huzimura and Atarashi (1982)
$CaSO_4$:Tm	300	2.0020, 2.0030, 2.0040 (II)	Huzimura and Atarashi (1982)
$CaSO_4$:Tm	300	2.0060, 2.0010 (III)	Huzimura and Atarashi (1982)
$CaSO_4$:^{241}Am	300	2.0030 (I)	Sheshagiri *et al* (1988)
$CaSO_4$:^{241}Am	77	2.0034 (II)	Sheshagari *et al* (1988)
$CaSO_4$:Dy, Na	300	2.0035, 2.0030, 2.0025	Gundu Rao *et al* (1993)

at 383 K. It is, therefore, likely that the SO_4^- (B) centre may be related to the TL peaks observed around the 383 K temperature range.

The line shape of the SO_4^- (A) radical at room temperature points to a small deviation from an isotropic g tensor towards an axially symmetric g tensor. It is seen from the variable-temperature experiment that the ESR signal of the SO_4^- (B) radical appears almost at the same position as SO_4^- (A) and the location is such as to give rise to the above-mentioned line shape. As the SO_4^- (B) radical decays completely at 150 °C, the sample was heated to 175 °C and the resulting ESR spectrum is shown in figure 10. It is seen that a slight axial symmetry still persists in the ESR spectrum of the SO_4^- (A) radical. These experiments show that the SO_4^- (A) radical is indeed characterized by an axially symmetric g tensor with $g_\parallel = 2.0104$ and $g_\perp = 2.0107$.

As mentioned earlier, there are several lines in ESR spectrum of irradiated $CaSO_4$:Eu (sample D-400, figure 5). The lines labelled B and C in the ESR spectrum of figure 5 occur in the region of $g = 2.0023$. These lines correspond to two distinct radicals. This

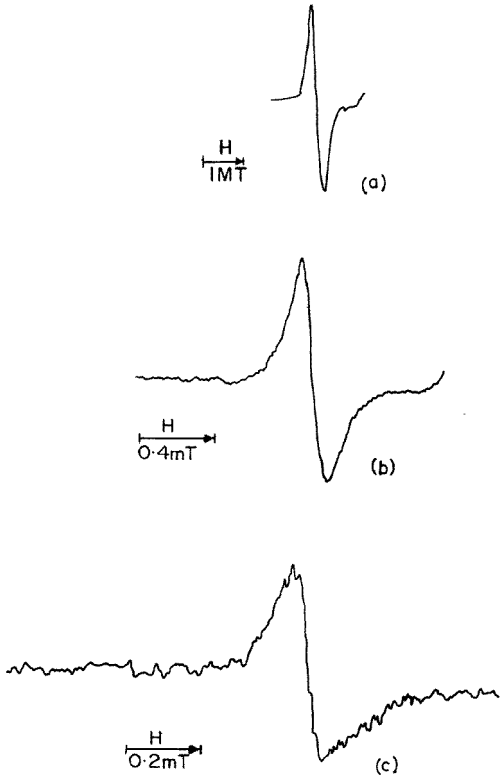

Figure 10. The ESR spectra of the SO_4^- radical at room temperature (a) in pure $CaSO_4$ powder (Huzimura 1979) and (b, c) in $CaSO_4$:Eu (b) before anneal and (c) annealed at 448 K (present study).

conclusion is based on the temperature variation of the ESR signal. Line B corresponds to a radical characterized by an axially symmetric tensor with principal values $g_\parallel = 2.0023$ and $g_\perp = 2.0055$ whilst the other radical has the principal values $g_\parallel = 2.0028$ and $g_\perp = 2.0056$.

The radical SO_3^- has been observed in pure and doped $CaSO_4$ and table 3 shows the principal g values of SO_3^- in these systems. The g factor of SO_3^- has been reported to be nearly isotropic, e.g. 2.0039 for $(NH_4)_2SO_4$ (Bailey and Cuesta-Barro 1975) and 2.0039 for $K_2CH_2(SO_3)_2$ (Chantry *et al* 1962). As the average g values of the centres associated with lines B and C (figure 5) are close to 2.0036, the two centres are assigned to SO_3^- radicals. The centre associated with line B is labelled as SO_3^- (A) while the centre corresponding to line C is labelled as SO_3^- (B). Step annealing measurements show that SO_3^- (A) decays in the temperature range 523–623 K. On the other hand, SO_3^- (B) is found to decay in the temperature range 513–643 K. As the onset of the release of charges from these centres starts from 523 K, it is likely that 560 K peak in the $CaSO_4$:Eu system may be caused by the electrons released from these two SO_3^- (B) defect centres.

The variable-temperature experiment in the low-temperature region showed that a new radical, not observed at ambient temperatures, beings to appear at 243 K. Figure 11(a) shows the ESR spectrum of this radical. The spectrum may be understood in terms of a radical with an axial g tensor where the unpaired electron interacts with two equivalent cations with nuclear spin $I = \frac{1}{2}$. Figure 11(b) shows a simulated spectrum with two equivalent

nuclei with nuclear spin $I = \frac{1}{2}$. The principal g values are found to be $g_{\parallel} = 2.0017$ and $g_{\perp} = 2.0062$. As ^{40}Ca (99.9% abundance) has nuclear spin $I = 0$, the observed splitting cannot be understood in terms of calcium cation interaction. However, the observed hyperfine interaction may be explained as due to the presence of traces of cations (with nuclear spin $I = \frac{1}{2}$) in the host lattice. The possible presence of such impurities in $CaSO_4$ host lattice cannot be ruled out as a contaminant. The observed principal hyperfine couplings are $A_{\parallel} = 178.6$ MHz and $A_{\perp} = 89.6$ MHz. These values indicate that the hyperfine interaction is nearly dipolar in character. Hence the hyperfine couplings are decomposed into an isotropic coupling constant A_{iso} and anisotropic coupling constant τ by assuming the maximum coupling ($A_{\parallel}$) to be positive and the other two values ($A_{\perp}$) negative. The isotropic coupling constant A_{iso} is found to be 0.2 MHz while the anisotropic coupling values are 178.8, -89.4 and -89.4 MHz. This radical is also assigned to SO_3^-, referred to as SO_3^- (C).

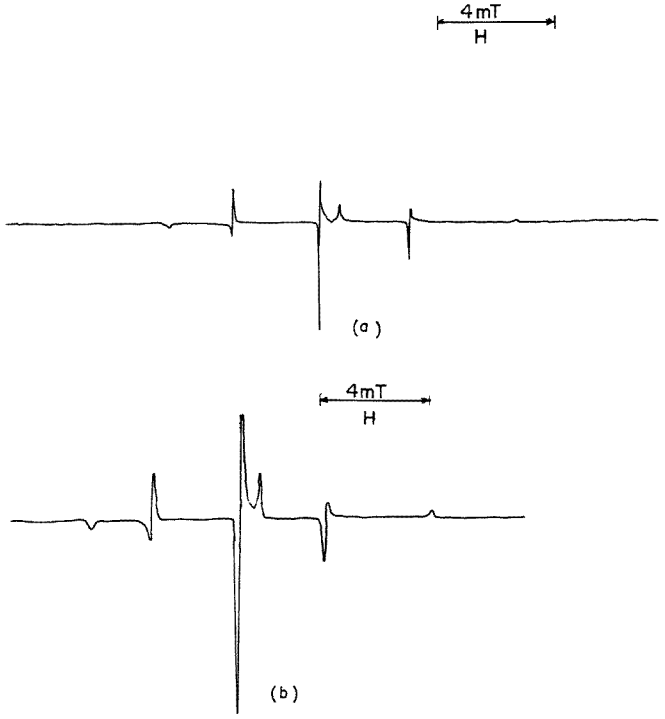

Figure 11. (a) The ESR spectrum of the SO_3^- (C) radical in $CaSO_4$:Eu recorded at 173 K and (b) a simulated spectrum assuming interaction with two equivalent cations with nuclear spin $I = \frac{1}{2}$.

The thermal decay of the ESR signal of SO_3^- (C) shows that this centre also starts decaying from 523 K. Consequently, SO_3^- (C) along with SO_3^- (A) and SO_3^- (B) appears to be related to the 560 K peak in the $CaSO_4$:Eu system.

Summarizing, earlier studies of pure $CaSO_4$ (Huzimura 1979) and Dy doped $CaSO_4$ (Morgan and Stoebe 1990) have shown that a variety of defect centres can be taped in this lattice. In the present study, three distinct defect centres could be identified in the room-temperature ESR spectrum of gamma irradiated $CaSO_4$:Eu system. One of these centres

has been assigned to SO_4^- (labelled as SO_4^- (A)) and the other two centres to SO_3^- (labelled as SO_3^- (A) and SO_3^- (B)). A noteworthy feature of the SO_4^- (A) radical in the $CaSO_4$:Eu system is the nearly isotropic nature of the g tensor. Such a feature has been observed only in pure $CaSO_4$. In the present study, it has been possible to give a qualitative explanation of this feature on the basis of an orbital level scheme.

Two additional defect centres have been observed at low temperatures. One of the centres has been assigned to SO_4^- (labelled as SO_4^- (B)). The other low-temperature radical is characterized by a hyperfine interaction with two equivalent cations with nuclear spin $I = 2$. This centre has been assigned to SO_3^- (labelled as (SO_3^- (C)).

The TL glow peak at 383 K appears to be related to the low-temperature SO_4^- (B) centre, while the 413 K peak is related to the SO_4^- (A) centre. On the other hand, it is particularly interesting to note that the high-temperature peak in $CaSO_4$:Eu at 560 K appears to arise from charges released from only SO_3^- centres (SO_3^- (A), SO_3^- (B) (room-temperature centres) and SO_3^- (C) (low-temperature centre)).

Various types of radical which could be present in irradiated $CaSO_4$:Eu have been described above. The relative concentrations of various radicals depend on the method of preparation and the type of irradiation (gamma or UV). SO_4^- radicals were observed only in the samples P-700 (containing predominantly Eu^{2+}). In D type samples, no SO_4^- radicals were found, but the dominant hole centres were SO_3^- (B) for gamma irradiation, while both SO_3^- (A) and SO_3^- (B) were present in the UV irradiated samples. In contrast, in $CaSO_4$:Dy, TL related centres corresponded to SO_4^- radicals.

Besides, hole trapped centres related to radicals, Eu^{2+} could also have been studied by ESR measurements. However, concentration of Eu^{2+} in all the samples was quite small and no ESR signals were detected which could be attributed to Eu^{2+}.

4. Conclusions

From the results presented and discussed the following can be concluded.

(i) Solubility of Eu in $CaSO_4$ is limited and not more than 0.05 mol% Eu can be doped without causing aggregation.

(ii) Radiation induced $Eu^{3+} \rightarrow Eu^{2+}$ conversion, and thus the intensity of RPL, increases with Eu concentration up to 50 ppm. Above this concentration increase in RPL is small.

(iii) For high Eu concentration and low pre-anneal temperature, a considerable fraction of Eu remains undissolved. Irradiation breaks the aggregates and produces Eu^{2+}. However, Eu^{2+} obtained by radiation induced reduction of Eu^{3+} can only be back-converted after post-irradiation thermal annealing. The origin of residual Eu^{2+} in the irradiated + annealed samples can be traced to the presence of undissolved Eu. For obtaining reusable samples in RPL dosimetry, samples with well-dispersed impurity will be necessary.

(iv) The mechanism of TL seems to be different for gamma irradiation than for UV irradiation. Model II explains the former while model I involving redox reactions $Eu^{3+} \leftrightarrow Eu^{2+}$ seems to be applicable to the latter.

(v) Various types of trapped hole centre such as SO_4^- and SO_3^- may be created in $CaSO_4$:Eu. The relative concentration of various centres depends on the method of preparation and the type of irradiation. A detailed description of the hole centres has been provided.

Acknowledgments

We are grateful to Professor P L Khanna, Director, NEERI, and Professor Lala, Director, RSCI, IIT, Powai, for granting permission to undertake these investigations.

References

Atkins P W and Symons M C R 1967 *The Structure of Inorganic Radicals* (Amsterdam: Elsevier)
Atone M S, Dhoble S J, Moharil S V, Dhopte S M, Muthal P L and Kondawar V K 1993a *Radiat. Eff. Defects Solids* **127** 225
——1993b *Phys. Status Solidi* a **135** 299
Ayyangar K, Chandra B and Lakshmanan A R 1974 *Phys. Med. Biol.* **19** 656
Azorin J, Furetta C and Sccaco A 1993 *Phys. Status Solidi* a **138** 9
Bailey C E and Cuesta-Barro R C 1975 *J. Chem. Phys.* **63** 4120
Bapat V N 1977 *J. Phys. C: Solid State Phys.* **10** L465
Bishop D M, Randic M and Morton J R 1966 *J. Chem. Phys.* **45** 1880
Calvert R L and Danby R J 1984 *Phys. Status Solidi* a **83** 597
Chantry G W, Horsfield A, Morton J R, Rowlands J R and Whiffen D H 1962 *Mol. Phys.* **5** 233
Danby R J 1983 *J. Phys. C: Solid State Phys.* **16** 3573
——1988 *J. Phys. C: Solid State Phys.* **21** 485
Danby R J, Boas J F, Calvert R L and Pilbrow J R 1982 *J. Phys. C: Solid State Phys.* **15** 2483
Danby R J and Mason N B 1984 *J. Chem. Phys.* **81** 5462
Dewar M J S and Thiel W J 1977 *J. Am. Chem. Soc.* **99** 4899
Dhopte S M, Muthal P L, Kondawar V K and Moharil S V 1991a *Radiat. Eff. Defects Solids* **117** 337
——1991b *J. Lumin.* **50** 187
——1992 *J. Lumin.* **54** 95
Gundu Rao T K, Bhatt B C, Srivastava J K and Nambi K S V 1993 *J. Phys.: Condens. Matter* **5** 1791s
Huzimura R 1979 *Japan. J. Appl. Phys.* **18** 2031
Huzimura R, Asahi K and Takenaga M 1980 *Nucl. Instrum. Methods* **175** 8
Huzimura R and Atarashi K 1982 *Phys. Status Solidi* a **70** 649
Iyer R K, Gokhale Y W, Gupta S K, Deshpande S G and Gupta S S 1980 *Dept. Atom. Energy Report* BARC I-591
Johansen H 1974 *Theor. Chim. Acta.* **32** 273
Merz J L and Pershan P F 1967a *Phys. Rev.* **162** 217
——1967b *Phys. Rev.* **162** 235
Morgan M J and Stoebe T G 1986 *Radiat. Prot. Dosim.* **17** 455
——1989 *J. Phys.: Condens. Matter* **1** 5773
——1990 *J. Phys.: Condens. Matter* **2** 1619
Nambi K S V, Bapat V N and Ganguly A K 1974 *J. Phys. C: Solid State Phys.* **7** 4403
Natarajan V, Dalvi A G I and Sastry M D 1988 *J. Phys. C: Solid State Phys.* **21** 5913
Prokic C 1978 *Nucl. Instrum. Methods* **51** 603
Samoilovich M I, Novozhilov A I, Bernov L V and Andrusenko N I 1968 *Radiokhimiya* **10** 506
Sheshagiri T K, Dalvi A G I and Sastry M D 1988 *J. Phys. C: Solid State Phys.* **21** 5891
Upadeo S V, Gubduaro T K and Moharil S V 1984 *J. Phys.: Condens. Matter* **6** 9459
Upadeo S V and Moharil S V 1995 *J. Phys.: Condens. Matter* **7** 957
——1997 *J. Phys.: Condens. Matter* **9** 735
Yamashita T 1974 *Proc. 4th Int. Conf. on Luminescence Dosimetry (Krakow, 1974)* (Krakow: Polish Academy of Sciences) p 467
Yamashita T, Nada N, Ohnishi H and Kitamura S 1968 *Proc. 2nd Int. Conf. on Luminescence Dosimetry (Gatlinburg)* p 4
——1971 *Health Phys.* **21** 253